

# Performance comparison of photocatalysts for degradation of organic pollutants using experimental studies supported with DFT and fundamental characterization

Nandana Chakinala<sup>a,c</sup>, Prabhat Ranjan<sup>b</sup>, Anand G. Chakinala<sup>a</sup>, Parag R. Gogate<sup>c,\*</sup>

<sup>a</sup> Chemical reaction engineering laboratory, Department of Chemical Engineering, Manipal University Jaipur, Dehmikalan, Jaipur 303007, Rajasthan, India

<sup>b</sup> Department of Mechatronics, Manipal University Jaipur, Dehmikalan, Jaipur 303007, Rajasthan, India

<sup>c</sup> Department of Chemical Engineering, Institute of Chemical Technology, Mumbai 400019, Maharashtra, India

## ARTICLE INFO

### Keywords:

Photocatalysis  
Bi-metallic catalysts  
PNP degradation  
Oxidants  
DFT computations

## ABSTRACT

The effect of different metal supported TiO<sub>2</sub> catalysts on the photocatalytic degradation of p-Nitrophenol (PNP) was investigated experimentally and supported by Density Functional Theory (DFT) approach. Process optimization studies were carried out using the best performing catalyst and the effect of different electron acceptors was also investigated. Degradation was strongly influenced by operating parameters and oxidants with efficacy as H<sub>2</sub>O<sub>2</sub> > K<sub>2</sub>S<sub>2</sub>O<sub>8</sub> > air. DFT simulations confirmed higher electrostatic potential in presence of hydroxyl radicals explaining the higher degradation. Overall, this work clearly establishes the effectiveness of electron acceptors in maximizing PNP degradation and explains the interaction of organic pollutants with different radicals.

## 1. Introduction

Ensuring the availability of clean water and sanitation is listed as one of the sustainable development goals by the United Nations [1]. At present, 40% of the world population is affected by the scarcity of drinking water and around ~80% of the polluted water being discharged into the atmosphere is driving the concerns further. Among the several existing technologies available for the treatment of polluted water, heterogeneous photocatalytic process is widely known for its cost-effective treatment [2,3]. The photocatalyst is vital in this process for the generation of e<sup>-</sup>/h<sup>+</sup> based on the absorption of light that splits the water molecule to produce hydroxyl radicals. These highly reactive radical species decomposes the organic pollutants present in the water by scissioning their bonds first to intermediates and finally to carbon dioxide. A lot of research in this field is mainly focused on the development of new materials that are able to work under visible light conditions and also in improving the performance of the catalyst with good activity and stability [4–8]. In addition, studies are also focussed in improving the degradation efficiency in the presence of different additives that act as electron acceptors/oxidizing agents. These additives can have a synergistic effect in terms of enhancing the hydroxyl radical production, reducing the recombination rate, and the production of

other oxidizing species [9,10].

A great deal of materials has been studied and reported in the literature for the photocatalytic degradation of organic pollutants in water but from a commercial perspective, TiO<sub>2</sub> based catalysts are more feasible due to their low cost, high activity, and abundant availability. We now present analysis of recent literature focusing on modifications in TiO<sub>2</sub> and its application for wastewater treatment to highlight the novelty of the planned work. In a recent study, monometallic bismuth doped TiO<sub>2</sub> was reported to be efficient for the degradation of methylene blue when compared with bimetallic Bi-Fe/TiO<sub>2</sub> [11]. In another study, bimetallic Bi-Zn/TiO<sub>2</sub> was reported to exhibit highest photocatalytic activity for the degradation of nitrobenzene [12]. CdTe nanoparticles modified TiO<sub>2</sub> nano tube arrays were reported to show enhanced photocatalytic activity for PNP degradation due to the effective separation of charge carriers and narrow band gap energies [13]. Ternary hybrid photocatalysts based on Sr<sup>2+</sup>/Ag-TiO<sub>2</sub>@rGO have also been reported to offer a synergistic effect between Ag, Sr<sup>2+</sup> and TiO<sub>2</sub> on the rGO surface having localized surface plasmon resonance (SPR) effect improving the charge transfer resulting into high catalytic activity [14]. GO/TiO<sub>2</sub> composite was elucidated to be a promising material for the degradation of salicylic acid under visible light conditions with enhanced charge transfer and reduced recombination rate [15]. Noble metal doped TiO<sub>2</sub>

\* Corresponding author.

E-mail address: [pr.gogate@ictmumbai.edu.in](mailto:pr.gogate@ictmumbai.edu.in) (P.R. Gogate).

<https://doi.org/10.1016/j.catcom.2022.106589>

Received 9 October 2022; Received in revised form 10 December 2022; Accepted 12 December 2022

Available online 13 December 2022

1566-7367/© 2022 The Authors. Published by Elsevier B.V. This is an open access article under the CC BY-NC-ND license (<http://creativecommons.org/licenses/by-nc-nd/4.0/>).

catalysts with Pt and Ag was investigated for the dichloroacetic acid degradation and it was reported that the hydroxyl radicals generated by  $O_2$  radical transformation are the major species involved in the degradation. Further,  $TiO_2/Ag$  junction was reported to generate Schottky barrier which enabled the transfer of electrons providing them for effective degradation [16]. Z-scheme  $TiO_2/Ta_3N_5$  heterojunction developed by a combination of defect engineering and heterostructure construction was reported to generate more photogenerated carriers, showing excellent activity for ciprofloxacin degradation [17]. Several advanced  $TiO_2$  based modified photocatalytic materials such as heterostructures [6,8,18], nanocomposites, metal doped [11,19–22] were also developed and applied for degradation of several hazardous pollutants [21,23–25]. Studies reported till date have used large amounts of catalyst, longer reaction times with expensive metal doping and stringent synthesis procedures. In the current work, an attempt has been made to develop cheaper and efficient catalysts for the degradation of different organic pollutants.

Intensifying the degradation and reducing the treatment time can be an important objective for the many additives applied in the wastewater treatment. The presence of additives such as air,  $O_2$ ,  $H_2O_2$ ,  $CCl_4$ , persulfate, and monosulfate in the system can stimulate the production of oxidizing species/free radicals in the system intensifying the overall degradation process [26–28]. Mishra and Gogate explored the effect of various additives for PNP degradation and concluded that  $CCl_4$  addition in optimum amount resulted in the maximum degradation with significant intensification [10]. In another work, optimum addition of  $H_2O_2$  was reported to accelerate the degradation of 2-methyl-4-chlorophenoxyacetic acid (MCPA) via increased OH radical production [29]. Sulfate radicals generated from additives such as persulfate (PS), peroxymonosulfate (PMS), and peroxydisulfate (PDS) have also been reported to drive the oxidation leading to intensified degradation of various organic pollutants in wastewater [12,20,30–32]. For example, beneficial effects of persulfate addition over Al-doped  $TiO_2$  with respect to degradation rate of propylparaben was attributed to the persulfate action as electron acceptor and source of extra radicals [20]. Bezafibrate degradation using a combination of Pd/g- $C_3N_4$  and PMS demonstrated enhancement in the removal efficiency in the presence of PMS owing to its capability of acting as electron acceptor, thereby increasing the quantum efficiency of the charge carriers to form sulfate radicals [30].  $Bi_2O_3/CuNiFe$  LDHs composite was reported to be effective for the effective degradation of lomefloxacin in the presence of persulfate which acted as an electron acceptor that hinders the recombination rate [31]. Further, theoretical studies such as molecular dynamic simulations (MD) and DFT have been used as tools in several studies to predict the material properties (band gap, charge transfer and distribution), so as to understand the experimental mechanism and to figure out the pollutant material interactions etc. For example, MD simulation carried out for adsorption of toxic metal ions of  $Cr^{3+}$  and  $Cd^{2+}$  on layered double hydroxide materials elucidated the adsorption behaviour and mechanism of metal ion adsorption that helped in demonstrating the efficacy of the novel material design [33]. Similarly, another study analyzed the adsorption of Pb(II) on the L-lysine (Lys) modified montmorillonite (L-Mt) using experimental investigations and MD simulations to understand the interaction properties of Lys and L-Mt and elucidated the adsorption mechanism occurring at water/clay minerals interface at atomic level [34]. In another study, DFT studies were carried out for degradation of diclofenac using quantum dots modified g- $C_3N_4$  so as to explain the probable sites of radical attack and intermediate formation [35].

The present study is an effort to investigate the photocatalytic efficiency of the bimetallic Ag–Bi doped  $TiO_2$  catalyst at varied metal loadings, for the degradation of organic pollutants. To further elucidate the degradation behaviour of this photocatalyst and the role of additives in the possible intensification of treatment process, theoretical first principal studies using density functional theory (DFT) were also carried out. The studies reported till date in the literature mainly focussed on

improving the materials for enhancing the photocatalytic efficiency but not many supported with fundamental reasoning. DFT, a very useful first principal method, was used to optimize the molecule structures, calculate the energy gap, and gain insights into the behaviour of molecular structures under different conditions. Detailed studies were carried out with PNP, an important industrial pollutant as it is one of most important refractory pollutants present in industrial effluents. The combined approach of both theoretical and experimental studies is expected to pave the way for new and efficient photocatalyst development and its application for intensified wastewater remediation.

## 2. Experimental

In this work, several photocatalysts were synthesized via ultrasound assisted wet impregnation technique (US-WI). All the catalysts synthesized were characterized and tested for degradation of pollutants under UV irradiation.

### 2.1. Chemicals and materials

*p*-Nitrophenol (PNP) was procured from Sigma Aldrich. Other chemicals like ethanol, nitric acid, silver nitrate, bismuth subnitrate, and different organic pollutants such as Terephthalic acid (TPA), *m*-Dinitrobenzene (*m*-DNB), Potassium persulfate (KPS), and 4-amino phenol (AMP) were procured from Loba Chemie. Titanium dioxide, and Hydrogen Peroxide (30% solution) was procured from Merck life sciences Private Limited. All the chemicals were of synthesis grade with high purity (>98%) and used as received from the supplier. Distilled water was used in all the catalyst synthesis methods and RO water was used for the preparation of the solutions of pollutants required for degradation studies.

### 2.2. Catalyst synthesis methods

Catalysts with various metal loadings of bismuth and silver were prepared using ultrasound assisted wet impregnation procedure described in our previous work [22]. Five different catalysts synthesized with different metal loadings such as AgBi/ $TiO_2$ (0.5:0.5 wt%), 1 wt% Ag/ $TiO_2$ , 1 wt% Bi/ $TiO_2$ , AgBi/ $TiO_2$ (1:1 wt%), AgBi/ $TiO_2$ (2:2 wt%) were denoted as Cat-1, Cat-2, Cat-3, Cat-4 and Cat-5 respectively.

### 2.3. Experimental setup and procedure

The experimental studies were carried out in a 750 ml batch reactor and the detailed procedure for performing studies is described elsewhere [22]. The photocatalytic degradation of PNP was carried out using different catalysts, operating conditions and intensified with the addition of oxidants to determine the best conditions. The full wavelength scan of the PNP showed maximum absorbance at 398 nm and the absorbance data for all PNP samples was recorded at this wavelength. All the experiments were carried out at a pH of 7 (unless specified) and the temperature was maintained at  $25 \pm 3$  °C using ice cold water circulation. For pH studies, the pH of feed solutions was adjusted with dilute 0.1 M  $HNO_3$  or 0.1 M NaOH solutions as per the requirement. For the studies involving TPA, *m*-DNB, AMP, and Rh–B, the absorbance was recorded at 238, 241, 224, and 555 nm respectively for the analysis using UV-vis spectrophotometer.

The percentage degradation of PNP and the average turnover frequency (TOF) of the catalyst were calculated using eq. (1) and (2) respectively. The pseudo first order kinetic model was used to estimate the apparent rate constant as shown in eq. (3) by plotting  $-\ln(C/C_0)$  vs  $t$ , where,  $C_0$  and  $C$  are the initial concentration and concentration measured at time  $t$  respectively.

$$\text{Pollutant degradation (\%)} = \left(1 - \frac{\text{Pollutant concentration in sample, } C}{\text{Initial pollutant concentration, } C_o}\right) \times 100 \quad (1)$$

$$\text{Average TOF} = \left(\frac{\text{moles of pollutant degraded with UV light}}{\text{moles of metal}}\right) / \text{reaction time} \quad (2)$$

$$-\ln\left(C/C_o\right) = k_{app}t \quad (3)$$

#### 2.4. Analytical method

Gas Chromatography/Mass Spectrometry analysis was carried out to identify the intermediate products formed during the PNP degradation. For the GC/MS analysis, a 20 ml sample was extracted in 4 ml ethyl acetate in the presence of continuous stirring followed by settling. The extracted organic layer was dehydrated using anhydrous sodium sulphate. 1  $\mu$ L of the dehydrated sample was injected into GC/MS system (Shimadzu QP 2020) with Rxi5 Sil MS column in split mode. The column was operated in temperature programmed mode with initial holding at 50  $^{\circ}$ C for 2 min, subsequent increasing at 10  $^{\circ}$ C  $\text{min}^{-1}$  to 280  $^{\circ}$ C, and again held for 2 min. The degradation products were qualitatively analyzed with reference to the NIST mass spectral library database.

Liquid effluent samples obtained after the reaction were also analyzed using a HACH-DR6000 UV-Vis spectrophotometer for measuring the concentration of the pollutant species.

#### 2.5. Computational details

All DFT calculations were performed using Gaussian 16 package and the geometry optimization was carried out using default convergence criterion followed by locating the true minimum potential energy. In this work, different systems involving the combined treatment of organic pollutants with the electron acceptors were studied in terms of molecular electrostatic potential (MEP) and Natural Bond Order (NBO). All the electron acceptors studied were placed at the aromatic ring of the pollutant geometry.

MEP surfaces in general describes the charge distribution associated with the molecule and is relatively a useful descriptor in determining the potential sites of a molecule that is prone towards electrophilic, nucleophilic, and radical attacks. It also helps in understanding the cleavage of bonds leading to intermediate compounds in the presence of radicals. The MEP as denoted as  $V(r)$  is given as follows in eq. 4 [28].

$$V(\vec{r}) = \sum \frac{Z_A}{|\vec{R}_A - \vec{r}|} - \int \rho(\vec{r}') / |\vec{r}' - \vec{r}| d\vec{r}' \quad (4)$$

Where, the summation applies to all the nuclei A with charge  $Z_A$  and coordinate  $\vec{R}_A$ , while  $\rho(\vec{r}')$ , is the molecule electron density.  $V(r)$  is the potential exerted at the coordinate  $r$  by the nuclei and the electrons and its sign at any point indicates the dominant effects of nuclei or electrons.

Natural Bond Orbital (NBO) analysis was also used to investigate the possible charge transfer and donor-acceptor interactions in molecular systems. The analysis was carried out by estimating the series of second order perturbation energies  $E(2)$  that correspond to energetic consequence of charge transfer between orbitals of two molecules, for all the possible interactions between filled (donor) NBO's and empty (acceptor) NBO's. The electron delocalization energies between donor-acceptor ( $i \rightarrow j$ ) is estimated as given in Eq. (5) [28].

$$E(2) = \Delta E_{ij} = q_i \frac{F_{(ij)}^2}{\varepsilon_i \varepsilon_j} \quad (5)$$

Where  $q_i$  is the donor orbital occupancy,  $\varepsilon_i$ ,  $\varepsilon_j$  are orbital energies of diagonal elements and  $F(i, j)$  is the off diagonal NBO Fock matrix element.

### 3. Results and discussion

#### 3.1. Catalyst characterization

All the synthesized catalysts were characterized using various characterization techniques such as Diffuse Reflectance Spectra (DRS), photoluminescence (PL), X-ray powder Diffraction (XRD), Scanning Electron Microscopy (SEM) and X-Ray Photoelectron Spectroscopy (XPS). The important analytical observations are discussed in detail in the supporting information. The band gap energies of all catalysts were also estimated using the PL spectra and found to be in good agreement with the theoretical values from DFT as listed in Table 1. All the other characterization results and associated discussion has been presented in the supplementary information.

#### 3.2. Effect of different catalyst metal loadings

The effectiveness of using different metal loadings of silver and bismuth on titania for the photocatalytic degradation of PNP was studied using five different catalysts (Cat-1, Cat-2, Cat-3, Cat-4, and Cat-5). All the synthesized catalysts using ultrasound assisted wet impregnation process were tested for their photocatalytic activity towards degradation of *p*-Nitrophenol with results shown in Fig. 1.

It is evident from Fig. 1a that 62% PNP degradation with a rate constant of 0.0163  $\text{min}^{-1}$  was achieved in 60 min with  $\text{TiO}_2$ , while the single metal/bimetal doped on  $\text{TiO}_2$  enhanced the extent of degradation as well as rate of degradation compared to only  $\text{TiO}_2$ . Monometallic catalysts of Cat-2 and Cat-3 resulted in a higher degradation of 83% (rate constant 0.0307  $\text{min}^{-1}$ ) and 68% (rate constant 0.0196  $\text{min}^{-1}$ ) respectively in comparison to base  $\text{TiO}_2$ . Bimetallic catalysts as Cat-1, Cat-4 and Cat-5, further improved the degradation with maximum conversion of 86% and higher rate constant of 0.0351  $\text{min}^{-1}$  was attained using an optimum combination of  $\text{AgBi/TiO}_2(0.5:0.5 \text{ wt}\%)$ . The enhanced photodegradation achieved with Cat-1 can be due to the increased light absorption in the UV range as compared to other catalysts (Fig. S.1) and lower recombination rate of charges (Fig. S.2). Additionally, this can also be due to the surface plasmon resonance effect exhibited by the silver and bismuth doped on the titania surface.

Increasing the metal content from 0.5 wt% to 2 wt% resulted in a negative effect on the catalytic activity for the degradation. Although Cat-4 and Cat-5 has slightly lower calculated band gap values (Table.1), the photon absorption is lower as compared to Cat-1 (Fig. S.1). Based on the obtained results, further studies were performed with the best performing catalyst of  $\text{AgBi/TiO}_2(0.5:0.5 \text{ wt}\%)$ . Similar observations of enhanced photocatalytic activity were reported in the literature at optimum  $\text{Ag/TiO}_2$ ,  $\text{Bi/TiO}_2$  loadings beyond which a negative effect on photocatalytic activity is observed [36]. Monometallic and bimetallic  $\text{Ag}$ ,  $\text{Cu/TiO}_2$  catalysts were shown to have the highest photocatalytic activity for the degradation of C.I. acid orange 7 in which the optimum loadings of  $\text{Ag}$ ,  $\text{Cu}$  were found to be 1, and 0.03 mol% respectively. Increasing the silver content decreased the activity due to screening of the  $\text{TiO}_2$  surface from light absorption and decreased active sites on the catalyst [37]. Photocatalytic degradation of bisphenol A was studied by Rengaraj and Li in which enhanced photocatalytic activity was noticed with 1 wt%  $\text{Ag-TiO}_2$  catalyst when compared to  $\text{TiO}_2$  [36,38]. It was also reported that an optimum dopant level of 1.5 wt%  $\text{Bi-TiO}_2$  exists for the photocatalytic degradation of methyl-parathion and nitrate [19]. Comparison with the literature clearly revealed that optimum conditions are different confirming the importance of the current work.

Turn Over Frequency (TOF), a measure of active catalytic site efficiency was also calculated using Eq. (2). The influence of different metal catalysts on the degradation of PNP presented in terms of turnover frequency (TOF) and the rate constant is shown in Fig. 1b. Maximum TOF of  $\sim 40 \text{ h}^{-1}$  was obtained with Cat-1 and Cat-3 that had different metal loadings and the TOF values were found to reduce with increasing the metal loadings in the case of Cat-4 and 5. It is apparent from the

**Table 1**  
HOMO, LUMO structures and the energy gap analysis of different synthesized catalysts and PNP.

Catalyst	Catalyst Composition	HOMO-LUMO Energy Gap (eV)	Calculated Band gap (eV)	HOMO	LUMO
Cat-1	0.5%Ag-0.5%Bi/TiO <sub>2</sub>	2.94	3.14		
Cat-2	1% Ag/TiO <sub>2</sub>	1.80	3.15		
Cat-3	1% Bi/TiO <sub>2</sub>	2.00	3.13		
Cat-4	1%Ag-1%Bi/TiO <sub>2</sub>	2.94	2.84		
Cat-5	2%Ag-2%Bi/TiO <sub>2</sub>	2.94	2.84		
	PNP molecule	3.76			

figure that the trends of TOF and the rate constants are different. Although Cat-1 and Cat-3 had a similar TOF values they had a different rate constant, with Cat-1 showing a maximum rate and the Cat-3 showing lowest rate among all the catalysts studied. It is interesting that lowest TOF values were obtained with Cat 4 and Cat 5 though they were found to have a better rate constant compared to others. Generally, the reaction rate is mathematically calculated as a product of TOF and the active metal concentration and in our case this mismatch between the TOF and the rate is mainly due to the different molar concentrations of the bi-metallic (Ag and Bi) deposited on the catalyst surface.

### 3.2.1. Quantum computational studies of the catalytic materials

Computational chemistry techniques using Density Functional Theory (DFT) are successful in understanding the electronic properties of chemical species. These tools help in better understanding of the interactions of the catalysts with the contaminants leading to improved understanding of the degradation mechanism as well as aid in the development of efficient catalysts. DFT studies were carried out to analyse the electronic structure by calculating the projected density of states which provide the energy gap and helps in interpreting the effect of metal loadings on the band gap. Experimental results with high conversions were achieved with a metal loading of AgBi/TiO<sub>2</sub>(0.5:0.5 wt %) considered to be the optimum. The results for the energy gap (Highest Occupied Molecular Orbital (HOMO) – Lowest Unoccupied

Molecular orbital (LUMO) gap, band gap) along with the frontier orbitals of the catalysts studied are shown in Table 1. The HOMO – LUMO gap characterizes the molecular chemical stability in which the red colour represents the negative charge, and the green colour represents the positive charges associated with the material/molecule. The HOMO and LUMO indicates the electron donor and electron acceptor respectively. It can be observed from the table that the HOMO and LUMO electron density of all the catalysts are different. Among the several catalysts studied, the HOMO-LUMO gap of Cat-1, Cat-4, Cat-5 were found to be similar at 2.94 eV due to equal amounts of metal loadings on the TiO<sub>2</sub> surface and these values are within a difference of  $\pm 0.2$  eV with calculated values (from photoluminescence spectra). These minor differences in the energy gaps can be attributed to the synthesis methods used. However, for Cat-2 and Cat-3, these differences were found to be higher with a difference of  $\pm 1.3$  eV.

HOMO-LUMO electron density of PNP molecule shown in the table was found to be different with the electron density majorly located on the benzene ring having a gap of 3.76 eV that is slightly higher ( $\sim 0.8$  eV) than the gap of the catalysts (Cat-1, 4 and 5) studied. Enhanced PNP degradation with Cat-1 can be attributed to the thermodynamically stable structure of the metals on the support, promotion of the charge separation, and suitable energy gap for the photocatalytic oxidation compared to mono metal catalysts.

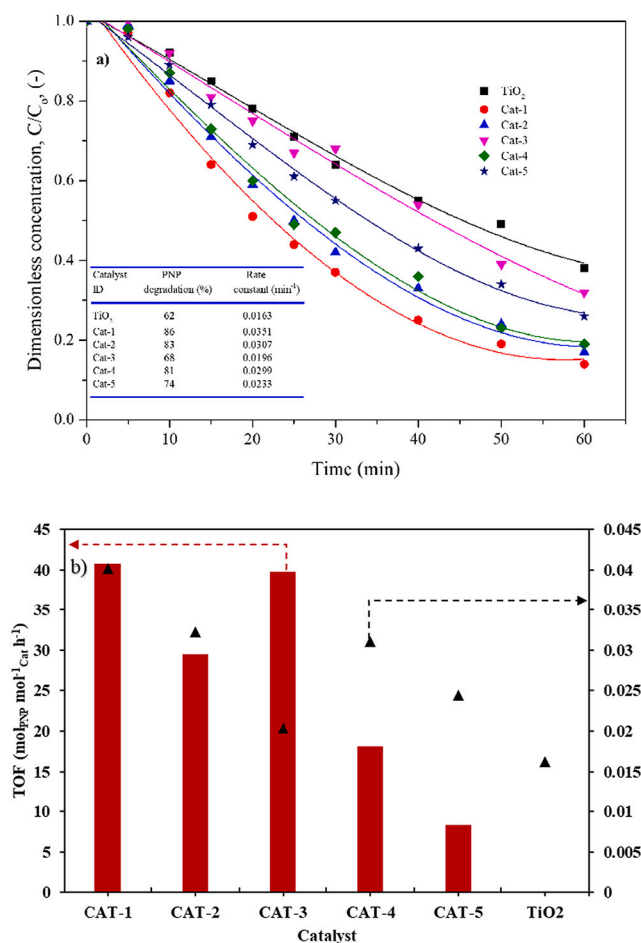


**Fig. 1.** a) Kinetics of degradation of PNP using catalysts having various metal loadings b) turnover frequency and the rate constants at different metal catalysts. [Experimental Conditions:  $T = 25\text{ }^{\circ}\text{C}$ , neutral pH, Lamp power – 250 W, feed concentration = 20 ppm, feed volume = 500 ml, Catalyst amount = 60 mg/L].

### 3.3. Effect of pH

It is known that the pH of feed affects the degradation and optimum value of pH is mainly dependant on the type of pollutants being treated. In this study, the initial pH of the feed solution was varied from acidic to basic conditions over the range of 3–10 to determine the optimum conditions of the treatment. The initial pH of the feed solution was adjusted using 0.1 M HNO<sub>3</sub> and 0.1 M NaOH as required. From the results shown in Fig. 2, it was found that at pH of 7, PNP was almost 90% degraded within 60 min and any change to pH > 7 or pH < 7 resulted in lower degradation of PNP. Thus, the optimum effective degradation of PNP was observed to occur under the neutral condition. It is known that the pKa value of PNP is 7.15 (@ 25 °C), and hence PNP exists in the molecular form at low pH and in the ionic form at high pH [39]. At higher pH of the feed solution, PNP decomposes to *p*-nitro phenoxide (ionic form) while at lower pH conditions, it remains in molecular form. Also, pH can cause the generation of charge at the catalyst surface. As the point of zero charge (PZC) for TiO<sub>2</sub> is  $\sim 6.2 \pm 0.1$ , at pH higher than the PZC, part of PNP that exists in ionic form will be repulsed by the catalyst surface. Thus the neutral conditions result in optimum balance for pollutant-catalyst interactions resulting in higher degradation. Liu et al. have also reported an optimum effect at pH of 6, with higher pH causing the electrostatic repulsion between sulphur modified ordered mesoporous carbon and PNP [40]. Therefore, as per results of current work, pH of  $\sim 6.5$  to 7 appears optimum considering the interaction of

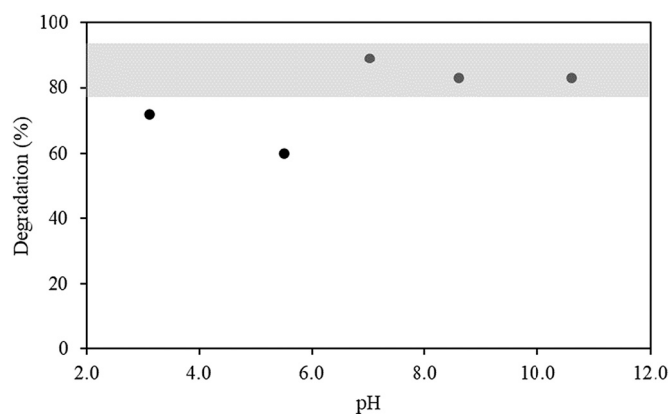


**Fig. 2.** Effect of pH on the degradation of PNP after 1 h treatment [Experimental Conditions: Temperature = 25 °C, feed concentration = 20 ppm; feed volume = 500 ml, lamp power = 250 W, catalyst amount = 60 mg/L, Catalyst type = Cat-1].

catalyst surface with the pollutant molecule. Considering the trend obtained in the current work, all the subsequent experiments were conducted at neutral conditions.

### 3.4. Effect of feed concentration

The effect of feed concentration on the degradation of PNP was investigated over the range of 20–80 ppm at a catalyst loading of 60 mg/l and the obtained results are presented in Fig. 3. It can be observed that extent of degradation decreased with an increase in the PNP concentration. The maximum extent of degradation as 96% was achieved for 20 ppm PNP solution with an apparent rate constant of  $0.0365\text{ min}^{-1}$ . Minimum degradation of 35% was obtained for the case of 80 ppm feed with a rate constant of  $0.00514\text{ min}^{-1}$ . The trends are likely due to the deposition of organic molecules on the catalyst surface which gets deactivated over a period. Moreover, as a definite amount of catalyst was used in all the experiments, the number of active sites on the catalyst are constant. As the ratio of catalyst to the feed concentration is reduced with increasing feed concentration, lower availability of active sites, also to some extent, plays a role in lowering the degradation as an optimum catalyst amount and the active sites is required for the photocatalytic process. Similar observations of lower degradation profiles

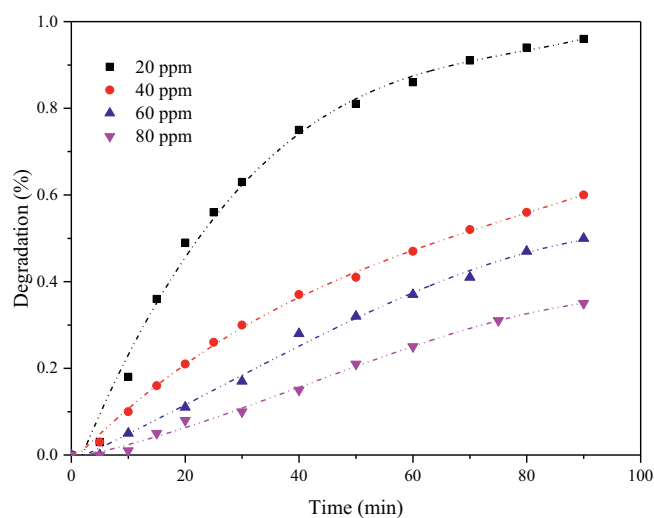


**Fig. 3.** Effect of feed concentration on the degradation of PNP. [Experimental conditions: Temperature = 25 °C, feed volume = 500 ml, lamp power = 250 W, Catalyst amount = 60 mg/L, Catalyst type = Cat-1].

with an increase in feed concentration have been reported in literature [9]. Increasing the PNP feed concentration from 10 mg/L to 50 mg/L reduced the rate constant from  $0.0226 \text{ min}^{-1}$  to  $0.011 \text{ min}^{-1}$  using a  $\text{Cu}_2\text{O}/\text{TiO}_2$  p-n heterojunction [8]. Mishra and Gogate also reported the decrease in extent of PNP degradation with increase in the initial concentration from 10 ppm to 100 ppm [9]. Sivakumar et al. studied the sonochemical PNP degradation and reported a decrease in the rate constant from  $1.33 \times 10^{-5} \text{ s}^{-1}$  to  $0.33 \times 10^{-5} \text{ s}^{-1}$  with an increase in concentration from 10 ppm to 500 ppm PNP solution [41].

### 3.5. Effect of lamp power

The lamp power plays a major role in deciding the economics of degradation of organic pollutants especially for a large-scale treatment process. It is desirable to operate with low lamp powers which reduces the power requirements and hence the cost of treatment. The effect of lamp power on the degradation of PNP was studied using lamps with different powers (25, 80 and 250 W). It was found that using lower powers of 25 and 80 W had a very little effect on the degradation (<10%) in 2 h irradiation when compared with 250 W where complete conversion was achieved within 90 min. This enhanced conversions at high lamp power is due to the higher absorption of photon energy. Similar lower extents of degradation of ~20% was also reported for a UV lamp of 11 W for a 10 ppm PNP solution after 240 min of irradiation time using  $\text{TiO}_2$  catalyst [9]. In a recent study, the effect of different lamp powers studied in the range of 200–600 W showed an increase in the degradation rate with increasing light intensity attributed to the generation of higher quantum of hydroxyl radicals [42]. Photocatalyzed degradation of 4-Chlorophenol was also studied using 8 W black lamp and 450 W Hg lamp and it was reported that low power lamps resulted in lower rates of degradation and lower rates of mineralization [43]. Cat-1 tested in our earlier work for different dyes in the visible light also showed a significant degradation and effective in converting the dyes at low power intensities but it was found to be difficult with highly recalcitrant pollutants such as PNP [22]. On the other hand, high lamp power was seen to result in significant degradation within 100 min of treatment in the same work. Comparison of the trends established that the trend depends on the type of pollutant and the range of power used making it essential to determine the optimum lamp power specific to organic effluent to be treated which may yield better results.

### 3.6. Degradation of different model pollutants

To study the effect of various functional groups on the aromatic rings on the levels of degradation, the photocatalytic activity of the catalyst was tested with various organic pollutants such as Rhodamine-B (Rh-B) dye, DNB, TPA, 4-AMP, and PNP. The results represented in Fig. 4 elucidate that the catalyst was active enough in completely degrading the Rh-B dye and PNP within 60 min of UV irradiation. In comparison to the organic pollutants with more functional groups on the aromatic rings, the degradation of dyes was more efficient with rates higher as compared to the other pollutants such as DNB or AMP. Under similar experimental conditions, the rate constant for the Rh-B dye degradation [22] was  $0.1176 \text{ min}^{-1}$  which is significantly higher than that of DNB and AMP ( $0.00525 \text{ min}^{-1}$  and  $0.00657 \text{ min}^{-1}$ ) respectively. In a similar trend, Se-ZnO incorporated with 3 wt% reduced graphene oxide was reported to completely mineralize methylene blue in 35 min with 0.2 g/L of catalyst in comparison to the time requirement of 105 min and 90 min for p-chlorophenol and p-nitrophenol respectively [7]. Several other dyes such as Methylene Blue (MB), Rhodamine-6G (Rh-6G), and Congo Red (CR) were also effectively degraded with the current catalyst as illustrated in earlier work [22]. The obtained results are attributed to the fact that the type of functional group has significant effect on the photocatalytic degradation. The aromatic rings consisting of nitro groups and amino group are more difficult to degrade than the aromatic ring with a hydroxyl group/carboxylic group. Similar observations of

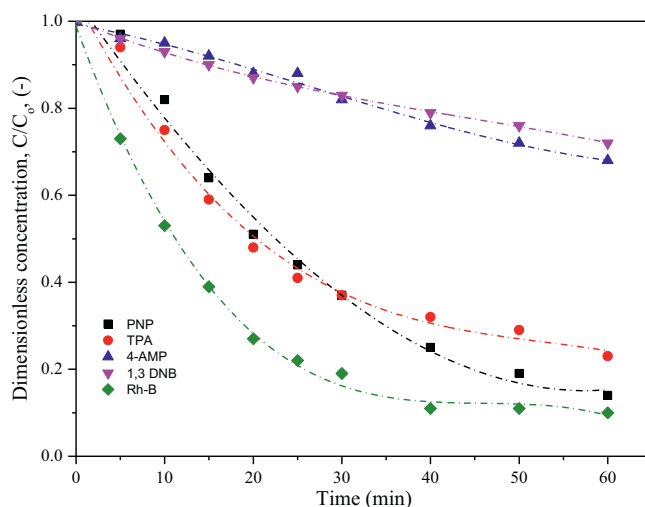


Fig. 4. Photocatalytic performance of Cat-1 for different model pollutants. [Experimental conditions: Temperature = 25 °C, neutral pH, feed concentration = 20 ppm, feed volume = 500 ml, lamp power = 250 W, Catalyst amount = 60 mg/L, Catalyst type = Cat-1].

the effect of various bi-functional aromatic rings and a slower *m*-DNB degradation was also reported in literature [44,45]. Photocatalytic degradation studies with *m*-DNB and NB showed complete degradation within 4 h and 2 h respectively and the lower rate with *m*-DNB was mostly due to its poor adsorption on the catalyst owing to its steric hindrance [44]. In another study, combustion synthesized nano  $\text{TiO}_2$  was applied for photocatalytic degradation of different functional group substituted benzene compounds and it was reported that the degradation rates followed the order: 1-chloro,2,4-dinitrobenzene >4-nitrophenol >2-nitrophenol >1-chloro,4-nitrobenzene >3-nitrophenol >2,4-dinitrophenol >1-chloro,2-nitrobenzene > nitrobenzene >1,3-dinitrobenzene. It was stated that the hydroxy substitution on the aromatic ring strongly activates the ring for the attack of electrophilic hydroxyl radicals and hence higher reactivity of nitrophenols is seen as compared to nitrobenzene [45].

The interaction between charge distributions of a pollutant molecule in the presence of the hydroxyl radicals generated in the system is shown in the form of MEP surface maps generated using DFT calculations in Fig. 5. It can be noticed that the magnitude of MEP calculated for different pollutants varies from low value ( $4.73 \times 10^{-2}$ ) for *m*-DNB and a high value ( $8.54 \times 10^{-2}$ ) for TPA. The red coloured regions/low value are indicative of attractive potential to a positive charge due to the relative abundance of electrons and blue coloured regions/high values are indicative of attractive potential to a negative charge due to the relative absence of electrons. Regions of positive electrostatic potential can result in attractive noncovalent interactions with the negative sites such as lone electron pairs and anions [46]. The degradation rates of the model compounds studied are in the order of Rh-B > PNP > TPA > 4-AMP ~ *m*-DNB. The surface charges as shown in Fig. 5 are also noticed to be in the same order as the experimental observations. The work is unique as majority of the earlier studies deal with only single pollutant and it is important to compare the results for different pollutants.

The results obtained in the current work also give a preliminary insight into the mechanistic pathways of the scission of the bonds in the presence of radicals and provides insights of possible intermediates that can be produced. Sites containing significant negative charges are more prone towards attack with the highly reactive radical species. Possible intermediates from TPA, or AMP degradation are hence reported to be benzoquinone, benzene, maleic acid, fumaric acid, oxalic acid etc., [47,48]. Similarly, possible intermediates from *m*-DNB degradation consists of resorcinol (RS), catechol, hydroquinone, benzoquinone, nitro hydroquinone, 4-nitrocatechol, phenol, 2,4-dinitrophenol and 3-

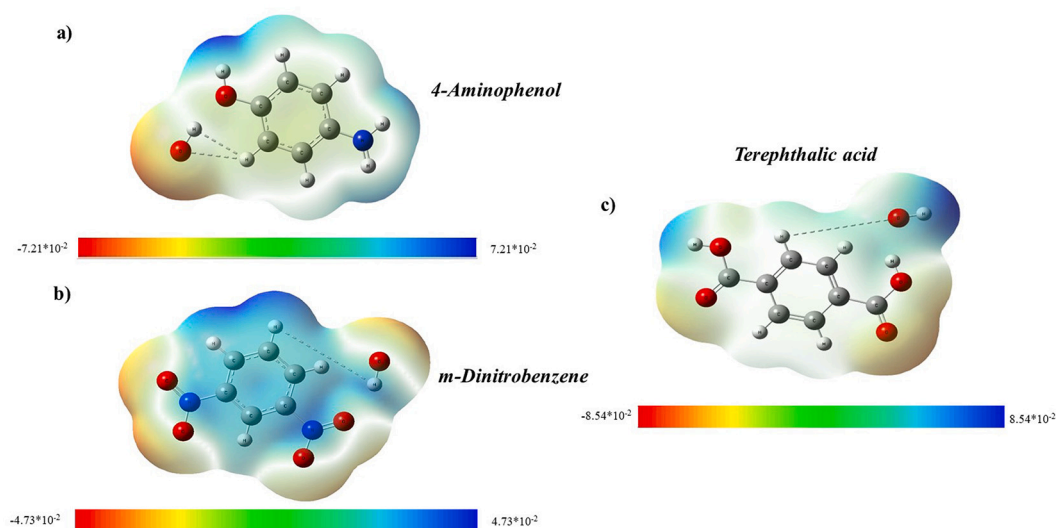


Fig. 5. Molecular electrostatic potential surface maps of the different pollutants studied in the presence of hydroxyl radicals a) 4-AMP b) m-DNB c) TPA.

nitrophenol [49].

### 3.7. Effect of electron acceptors on the degradation

The effect of addition of different electron acceptors such as air,  $\text{H}_2\text{O}_2$ , and  $\text{S}_2\text{O}_8^{2-}$  to the reaction system on the rate of PNP degradation is shown in Fig. 6a. These electron acceptors are known to enhance the formation of highly reactive radical species that can favour the degradation of organic pollutants. The addition of  $\text{e}^-$  acceptors also acts as  $\text{e}^-$  scavengers leading to reduced electron-hole recombination. From the figure, it is evident that the degradation of PNP in the absence of catalyst or electron acceptor was negligible, indicating that the direct photolysis of PNP alone was insignificant. Furthermore, all the other  $\text{e}^-$  acceptors were found to be effective in intensifying the degradation of PNP in the order of  $\text{H}_2\text{O}_2 > \text{K}_2\text{S}_2\text{O}_8 > \text{air}$ . The rate constants in the presence of air, persulfate addition and peroxide addition was found to be 0.00436, 0.01257,  $0.554 \text{ min}^{-1}$  respectively which is 1.2, 3.4 and 14.8 times higher than that seen for UV alone (actual value as  $0.003735 \text{ min}^{-1}$ ). The enhancement in the degradation rate with hydrogen peroxide addition is due to its dissociation to produce highly reactive hydroxyl radical species (reaction R1-R5) and the production of sulphate radicals accompanied with hydroxyl radicals (redox potential 2.8 V) in the case of potassium persulfate addition (reaction R6-R11) drives the intensification. It is known that the direct reaction of persulfate with many organic pollutants is rather slow and hence it needs activation via energy based or catalyst based processes to generate the stronger oxidizing potential sulphate radicals (redox potential 2.6 V) [50]. It was observed in the work that the enhancement in the PNP degradation in the presence of sulphate was lower as compared to the case of  $\text{H}_2\text{O}_2$  and hence no further investigations was carried out in determining the optimum sulphate concentration. In addition, it is imperative that the activated persulfate in the presence of catalyst, resulted in enhanced PNP degradation as compared to only UV based degradation which is very much similar to the results in the presence of hydrogen peroxide.

Intensified degradation rates were reported in the literature as well with the addition of different oxidants studied for several organic pollutants [30,51,52]. Higher removal efficiency of bezafibrate was reported with a rate constant of  $0.0098 \text{ min}^{-1}$  in the presence of peroxymonosulfate (PMS) and visible light as compared to  $0.0012 \text{ min}^{-1}$  in the absence of PMS [30]. Cyanotoxin microcystin-LR was also reported to degrade with higher efficiency with the addition of sulfate radical generating oxidants in which the PMS outperformed PS as PMS accepts electrons more easily [51]. Higher PNP degradation of 83%

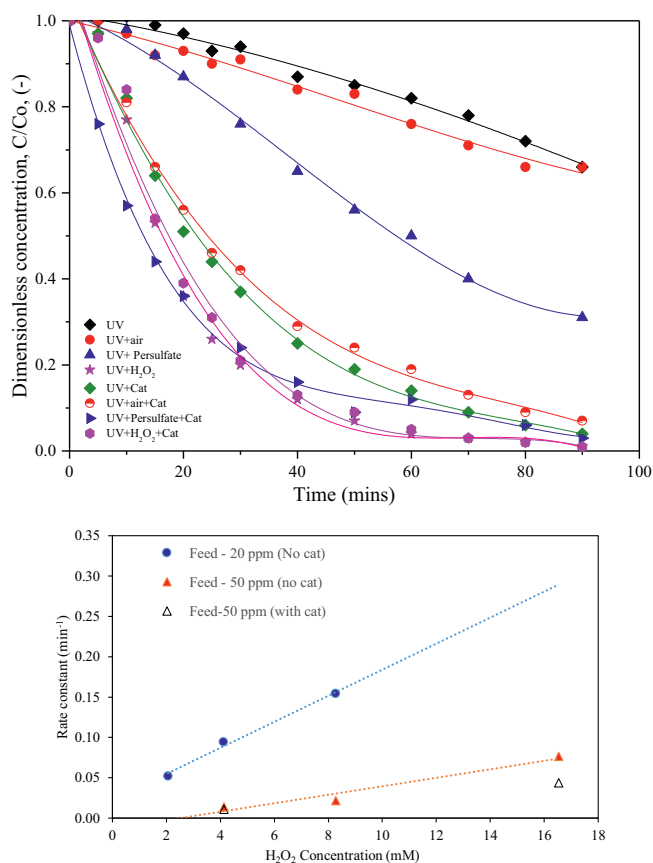
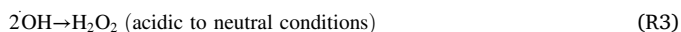


Fig. 6. a) Kinetics of photolytic/photocatalytic degradation of PNP in the presence and absence of different electron acceptors [Experimental conditions: Temperature =  $25^\circ\text{C}$ , neutral pH, feed concentration = 20 ppm, feed volume = 500 ml, lamp power = 250 W, Catalyst amount = 60 mg/L, Catalyst type = Cat-1,  $\text{H}_2\text{O}_2$  concentration = 2 mM, Persulfate concentration = 0.216 mM]. b) Influence of  $\text{H}_2\text{O}_2$  concentration on the rate constant.

within 60 min was reported in case of non-zero valent iron activated PS described by rapid formation of oxidizing species [53]. A synergistic effect between photocatalysis and peroxymonosulphate activation was reported with CoAl-LDH/BiOBr composite for the degradation of

ciprofloxacin [12]. Comparison with literature confirmed the quantitative differences in the extent of intensification as well as the best loading observed for oxidants clearly elucidating the importance of the current work.



However, the presence of a photocatalyst along with electron acceptor had no substantial effect on the rate constant with any of the electron acceptors studied as compared to the presence of photocatalyst alone. The addition of persulphate and hydrogen peroxide produces a complex effect when used in combination with photocatalysis as the respective generation of sulphate ions ( $\text{SO}_4^{2-}$ ) and hydroxyl ions ( $\text{OH}^-$ ) typically acts as a hole scavenger. Overall, this may lead to limited or no significant effect in the degradation process due to this trade-off in the presence of a photocatalyst and electron acceptor.

Further, to determine the optimum concentration of  $\text{H}_2\text{O}_2$ , tests were performed with different PNP concentrations (20 & 50 ppm) and with varied concentrations of  $\text{H}_2\text{O}_2$  (2–16 mM) with the results presented in Fig. 6b. It is seen that with an increase in the peroxide concentration the degradation efficiency was found to have an increasing linear trend, which is due to the production of highly reactive radical species generated from the dissociation of hydrogen peroxide with UV light. However, an optimum value of  $\text{H}_2\text{O}_2$  concentration is reported in

literature beyond which the degradation rate reduces [9,28]. Such optimum value of peroxide concentration was not noticed in the current study over the range of applied peroxide concentrations for both feed concentrations studied. Additionally, the observed higher rate constants with low feed concentration shown in Fig. 6b is line with the earlier observations discussed in section 3.3. An interesting observation was that the reaction rates were found to be lower in the presence of a catalyst for 50 ppm feed and higher peroxide dosages when compared with no catalyst. This is mainly due to the formation of peroxy compounds on the catalyst surface with the use of high dosages of hydrogen peroxide that are found to be detrimental in the photocatalytic reaction.

### 3.7.1. DFT insights

DFT computational analysis was also carried out to better understand the interactions between PNP and radicals generated in the system. Fig. 7 illustrates the interaction effects of the organic pollutant with different electron acceptors represented in the form of MEP surfaces of the investigated components. A transparent view of the molecule interaction with the electron acceptor encapsulated in an electron cloud with different colours is presented where the blue colour area corresponds to highest electrostatic potential and the red colour represent areas with lowest electrostatic potential. The MEP surfaces for systems with different radicals were found to have a significant change in their charge distribution. With the introduction of radicals, the minimum and maximum values varied significantly, and the associated change was highest with the  $\text{SO}_4^{\cdot -}$ . The location of the radicals bound to the aromatic ring is different in each of these cases having different charge distributions which indicate interesting chemical interaction between the sites of PNP and the studied radicals. The presented results give a preliminary insight into the mechanistic pathways of the scissioning of the molecule bonds in the presence of radicals and provides insights of possible intermediates that can be produced. This theoretical analysis closely matches with the literature [28] as well as our experimental observations for comparison of effectiveness of air, hydrogen peroxide and sulphate. It was clearly elucidated that maximum degradation was obtained with hydrogen peroxide followed by sulphate radicals when studies were performed in the absence of any catalyst due to very slow reaction of sulphate radicals with the organic pollutants.

The donor-acceptor interactions and charge transfer between orbitals was investigated using NBO analysis, in which the electron delocalization energies of all possible NBO orbital interactions are summated as  $\Sigma E(2)$  as shown in Table 2. Larger delocalization energies are indicative of strong interactions while smaller values are indicative of weak

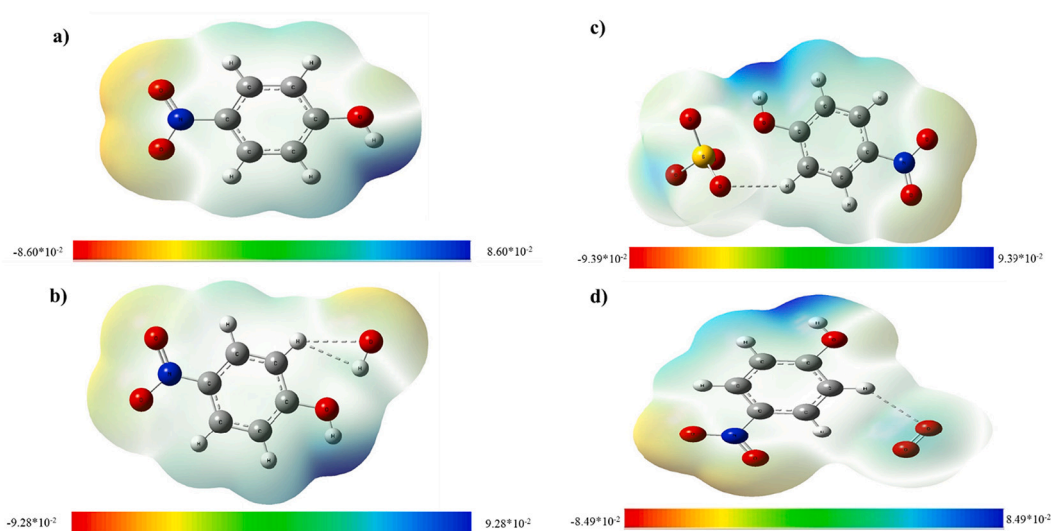


Fig. 7. Molecular orbital potential surfaces of the systems involving different oxidants a) PNP b) PNP with hydroxyl radical c) PNP with Sulphate and d) PNP with superoxide radicals.

**Table 2**  
 $\Sigma E(2)$  of interacting NBOs of PNP and radicals.

System	Donor unit (NBOs of)	Acceptor unit (NBOs of)	$\Sigma E(2)$ (kcal/mol)
PNP/ $O_2^-$	PNP	$O_2^-$	0.11
	$O_2^-$	PNP	8.11
PNP/ $\cdot$ OH	PNP	$\cdot$ OH	0.39
	$\cdot$ OH	PNP	18.87
PNP/ $SO_4^-$	PNP	$SO_4^-$	1.77
	$SO_4^-$	PNP	21.76

electrostatic interactions between the investigated molecules. As shown in Table 2, the significant chemical interactions took place between NBO of sulphate radicals to PNP followed by hydroxyl radicals to PNP as noticed from the  $\Sigma E(2)$  values of 21.76 and 18.87 respectively. While, the electron delocalization from PNP to any of the radicals generated in the system are found to be insignificant, as indicated by lower  $\Sigma E(2)$  values. These findings are consistent with the above observations of MEP surface plots in which a different charge distribution on PNP molecule was observed in the presence of sulphate radicals. Moreover, the findings are also consistent with the experimental observations of maximum PNP degradation with  $H_2O_2$  followed by persulphate in the absence of any catalyst, implying that the  $\cdot$ OH generated by  $H_2O_2$  dissociation and  $SO_4^-$  generated by persulphate dissociation contributed to the PNP degradation.

### 3.8. Reaction pathway

Fig. 8 shows a plausible reaction mechanism for the photocatalytic degradation of PNP in which initially the hydroxyl radicals or the sulphate radicals primarily attack the nitro group of the benzene ring producing phenol and nitro radicals. The phenol produced further undergoes oxidation with the residual free radicals and gets converted to other products such as hydroquinone. In addition, strong electrophilicity of hydroxyl radicals results in hydroxylation of the benzene ring forming

4-nitrocatechol [13,53]. Hydroxyl radical attack on PNP also produces benzoquinone and hydroquinone [13]. Among the several compounds shown in the scheme, a limited number of compounds were identified in this study such as the unconverted PNP (in significant quantities as the samples with lower conversion were analyzed specifically), phenol, hydroquinone, and carboxylic acids such as benzoic acid and propanoic acid. Although, several studies have reported the presence of benzoquinone, 4-nitrocatechol, and trihydroxy benzene, they were not identified in our samples which may possibly be due to its direct conversion to acids or may be these compounds are out of the detection limits.

### 3.9. Commercial relevance of the obtained results

The demonstrated results in terms of effectiveness of the silver bismuth doped titanium dioxide for degradation of variety of pollutants are definitely of commercial relevance. It is known that photocatalyst plays a vital role in deciding the degradation of pollutants present in the wastewater. From an industrial perspective, the catalyst must be effective, cheaper, and stable. The easy availability, low price of  $TiO_2$  makes the  $TiO_2$  based catalysts commercially attractive from the industrial application viewpoint. Use of lower metal loadings of active metals like silver and bismuth further enhanced photocatalytic activity that was confirmed with the experimental observations and theoretical calculations. The underlying mechanisms for catalyst activity and the role of electron acceptors are expected to be equally valid at commercial scale as well. Overall findings of the current work coupled with the stability and reusability studies reported for similar doped catalysts in our earlier study [22] for 5 consecutive cycles clearly elucidate the potential of doped catalysts for commercial exploitation.

## 4. Conclusions

The current study has demonstrated the enhanced photocatalytic activity of silver bismuth doped titanium dioxide at an optimum loading of 0.5 wt% of Ag and Bi for the degradation of PNP. Theoretical studies

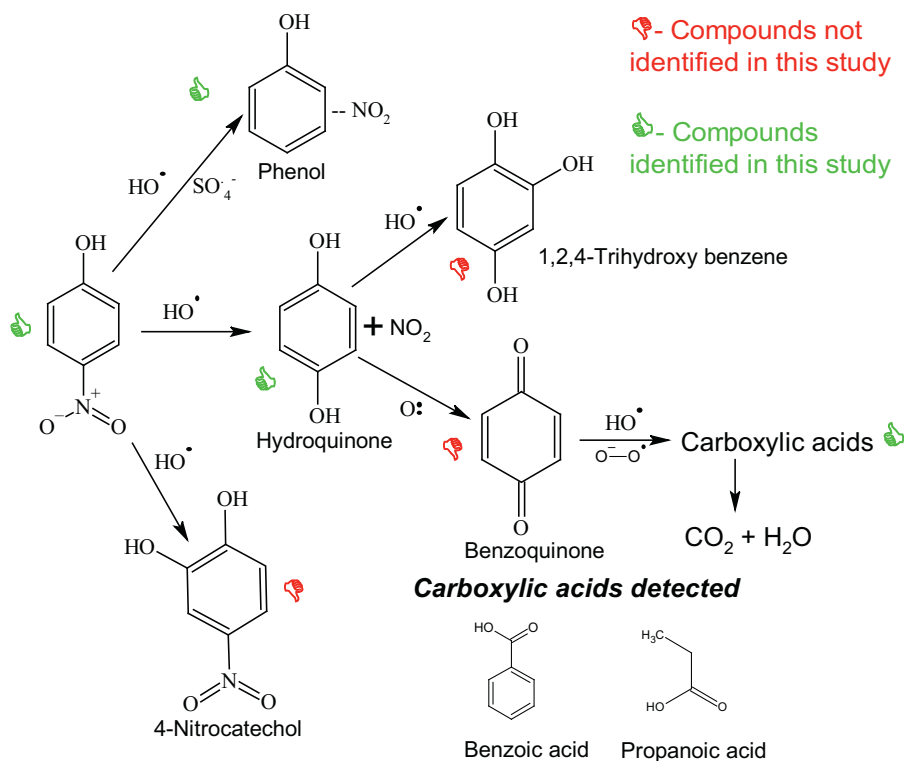


**Fig. 8.** Possible reaction pathway of the photocatalytic degradation of PNP.

using density functional theory also confirmed sufficient band gap of bimetallic catalysts for good photon absorption in line with the experimental observations of enhanced photocatalytic activity. Process optimization studies using the best catalyst was carried out at different pH conditions, and different initial feed concentrations which showed marginal effects of pH on the degradation and lower feed concentrations favouring higher degradation rates. In addition, studies with different lamp powers showed negligible effect for the degradation at low lamp powers and higher degradations at higher power studied. The best catalyst with 0.5 wt% Ag 0.5 wt% Bi supported on titania was found to be active enough for the degradation of various other pollutants such as Rh-B, TPA, m-DNB, 4-AMP. The role of various electron acceptors such as air, hydrogen peroxide, and potassium persulphate studied in terms of the degradation of PNP showed minimal/negligible role of oxygen in photocatalytic process whereas the addition of hydrogen peroxide and persulphate improved the degradation of PNP. It was found that the optimum concentrations of hydrogen peroxide resulted in 100% degradation within a shorter period of 30 min for a 20 ppm feed. For the case of persulphate addition, it was observed that rate almost increased by 3.5 folds as compared to direct photolysis. In addition, the activation of persulfate with catalyst resulted in the synergistic effect of higher degradation rates though lower as compared to the presence of H<sub>2</sub>O<sub>2</sub> in the system. Computational studies of molecular electrostatic potential using DFT also indicated higher electrostatic potential (0.0939) with hydroxyl radicals compared to sulphate and oxygen addition. NBO analysis suggested that hydroxyl and sulphate radicals generated in the system favour PNP degradation, and these theoretical predictions closely matched with the experimental observations of higher degradations with hydrogen peroxide than persulfate addition. Overall, this study systematically shown excellent photocatalytic activity for degradation of various organic pollutants in the presence of different oxidants with supporting evidence based on the theoretical predictions.

#### CRedit authorship contribution statement

**Nandana Chakinala:** Methodology, Investigation, Formal analysis, Writing – original draft. **Prabhat Ranjan:** Investigation, Methodology, Writing - review & editing. **Anand G. Chakinala:** Writing – review & editing. **Parag R. Gogate:** Supervision, Project administration, Writing - review & editing.

#### Declaration of Competing Interest

On behalf of all authors, the corresponding author states that there is no conflict of interest.

#### Data availability

Data will be made available on request.

#### Acknowledgements

The authors would like to thank Manipal University Jaipur (MUJ) for providing access to the Central Analytical Facilities (CAF) and Sophisticated Analytical Instrumentation Facility (SAIF). Authors also acknowledge the support of UGC Networking Resource Centre at Institute of Chemical Technology, Mumbai for enabling the PhD degree work.

#### Appendix A. Supplementary data

Supplementary data to this article can be found online at <https://doi.org/10.1016/j.catcom.2022.106589>.

#### References

- [1] United Nations Sustainable Development Goal, Goal-6, United Nations. <https://sdgs.un.org/goals/goal6>, 2022 (accessed August 23, 2022).
- [2] E. Kweiner Tetteh, S. Rathilal, M. Chetty, E. Kwaku Armah, D. Asante-Sackey, Treatment of water and wastewater for reuse and energy generation-emerging technologies, in: M. Eyyav (Ed.), *Water Wastewater Treat* (2019) 1–21, <https://doi.org/10.5772/intechopen.84474>.
- [3] N. Mohammed, P. Palaniandy, F. Shaik, Pollutants removal from saline water by solar photocatalysis: a review of experimental and theoretical approaches, *Int. J. Environ. Anal. Chem.* (2021) 1–21, <https://doi.org/10.1080/03067319.2021.1924160>.
- [4] C. Wang, J. Shen, R. Chen, F. Cao, B. Jin, Self-assembled BiOCl/Ti3C2Tx composites with efficient photo-induced charge separation activity for photocatalytic degradation of p-nitrophenol, *Appl. Surf. Sci.* 519 (2020), <https://doi.org/10.1016/j.apsusc.2020.146175>. Article ID 146175.
- [5] M. Tong, D. Sun, R. Zhang, H. Liu, R. Chen, Preparation of Si- $\alpha$ -Fe2O3/CdS composites with enhanced visible-light photocatalytic activity for p-nitrophenol degradation, *J. Alloys Compd.* 862 (2021), <https://doi.org/10.1016/j.jallcom.2020.158271>. Article ID 158271.
- [6] D. Sun, L. Jia, C. Wang, H. Liu, R. Chen, Preparation of the additive-modified  $\alpha$ -Fe2O3/g-C3N4 Z-scheme composites with improved visible-light photocatalytic activity, *J. Environ. Chem. Eng.* 9 (2021), <https://doi.org/10.1016/j.jece.2021.106274>. Article ID 106274.
- [7] S. Kumar, R.D. Kaushik, L.P. Purohit, Hetro-nanostructured Se-ZnO sustained with RGO nanosheets for enhanced photocatalytic degradation of p-chlorophenol, p-nitrophenol and methylene blue, *Sep. Purif. Technol.* 275 (2021), <https://doi.org/10.1016/j.seppur.2021.119219>. Article ID 119219.
- [8] L. Yang, S. Luo, Y. Li, Y. Xiao, Q. Kang, Q. Cai, High efficient photocatalytic degradation of p-nitrophenol on a unique Cu<sub>2</sub>O/TiO<sub>2</sub> p-n heterojunction network catalyst, *Environ. Sci. Technol.* 44 (2010) 7641–7646, <https://doi.org/10.1021/es101711k>.
- [9] K.P. Mishra, P.R. Gogate, Intensification of sonophotocatalytic degradation of p-nitrophenol at pilot scale capacity, *Ultrason. Sonochem.* 18 (2011) 739–744, <https://doi.org/10.1016/j.ultsonch.2010.11.004>.
- [10] K.P. Mishra, P.R. Gogate, Ultrasonic degradation of p-nitrophenol in the presence of additives at pilot scale capacity, *Ind. Eng. Chem. Res.* 51 (2012) 1166–1172, <https://doi.org/10.1021/ie2023806>.
- [11] S. Mishra, N. Chakinala, A.G. Chakinala, P.K. Suroliya, Photocatalytic degradation of methylene blue using monometallic and bimetallic Bi-Fe doped TiO<sub>2</sub>, *Catal. Commun.* 171 (2022), 106518, <https://doi.org/10.1016/j.CATCOM.2022.106518>.
- [12] C. Liu, S. Mao, M. Shi, F. Wang, M. Xia, Q. Chen, X. Ju, Peroxymonosulfate activation through 2D/2D Z-scheme CoAl-LDH/BiOBr photocatalyst under visible light for ciprofloxacin degradation, *J. Hazard. Mater.* 420 (2021), 126613, <https://doi.org/10.1016/j.jhazmat.2021.126613>.
- [13] M. Heibati, E. Jalilnejad, F. Vahabzadeh, Photocatalytic degradation of p-nitrophenol in an annular column photoreactor and the intermediates, *Water Environ. Res.* 87 (2015) 437–443, <https://doi.org/10.2175/106143015x14212658614234>.
- [14] X. Wei, J. Cao, F. Fang, A novel multifunctional Ag and Sr<sup>2+</sup> co-doped TiO<sub>2</sub>@rGO ternary nanocomposite with enhanced: P-nitrophenol degradation, and bactericidal and hydrogen evolution activity, *RSC Adv.* 8 (2018) 31822–31829, <https://doi.org/10.1039/c8ra06813e>.
- [15] Y.M. Hunge, A.A. Yadav, A.G. Dhodamani, N. Suzuki, C. Terashima, A. Fujishima, V.L. Mathe, Enhanced photocatalytic performance of ultrasound treated GO/TiO<sub>2</sub> composite for photocatalytic degradation of salicylic acid under sunlight illumination, *Ultrason. Sonochem.* 61 (2020), <https://doi.org/10.1016/j.ultsonch.2019.104849>. Article ID 104849.
- [16] P. Ribao, J. Corredor, M.J. Rivero, I. Ortiz, Role of reactive oxygen species on the activity of noble metal-doped TiO<sub>2</sub> photocatalysts, *J. Hazard. Mater.* (2019) 45–51, <https://doi.org/10.1016/j.jhazmat.2018.05.026>.
- [17] M. Li, J. Zhang, L. Wang, X. Cheng, X. Gao, Y. Wang, G. Zhang, Y. Qi, H. Zhai, R. Guan, Z. Zhao, Direct Z-scheme oxygen-vacancy-rich TiO<sub>2</sub>/Ta3N5 heterojunction for degradation of ciprofloxacin under visible light: degradation pathways and mechanism insight, *Appl. Surf. Sci.* 583 (2022), <https://doi.org/10.1016/j.apsusc.2022.152516>. Article ID 152516.
- [18] Y. Zhao, X. Linghu, Y. Shu, J. Zhang, Z. Chen, Y. Wu, D. Shan, B. Wang, Classification and catalytic mechanisms of heterojunction photocatalysts and the application of titanium dioxide (TiO<sub>2</sub>)-based heterojunctions in environmental remediation, *J. Environ. Chem. Eng.* 10 (2022), 108077, <https://doi.org/10.1016/j.jece.2022.108077>.
- [19] S. Rengaraj, X.Z. Li, Enhanced photocatalytic reduction reaction over Bi<sup>3+</sup>-TiO<sub>2</sub> nanoparticles in presence of formic acid as a hole scavenger, *Chemosphere* 66 (2007) 930–938, <https://doi.org/10.1016/j.chemosphere.2006.06.007>.
- [20] S. Kotzamanidi, Z. Frontistis, V. Binas, G. Kiriakidis, D. Mantzavinos, Solar photocatalytic degradation of propyl paraben in Al-doped TiO<sub>2</sub> suspensions, *Catal. Today* 313 (2018) 148–154, <https://doi.org/10.1016/j.cattod.2017.12.006>.
- [21] S. Preeti, N. Mishra, A.G. Chakinala, P.K. Chakinala, Suroliya, bimetallic Bi/Zn decorated hydrothermally synthesized TiO<sub>2</sub> for efficient photocatalytic degradation of nitrobenzene, *Catal. Commun.* 172 (2022), 106538, <https://doi.org/10.1016/j.CATCOM.2022.106538>.
- [22] N. Chakinala, P.R. Gogate, A.G. Chakinala, Highly efficient bi-metallic bismuth-silver doped TiO<sub>2</sub> photocatalyst for dye degradation, *Korean J. Chem. Eng.* 38 (2021) 2468–2478, <https://doi.org/10.1007/s11814-021-0890-5>.

- [23] A. Chakraborty, O. Samriti, R.K. Ruzimuradov, J. Gupta, J. Prakash Cho, TiO<sub>2</sub> nanoflower photocatalysts: synthesis, modifications and applications in wastewater treatment for removal of emerging organic pollutants, *Environ. Res.* 212 (2022), 113550, <https://doi.org/10.1016/j.envres.2022.113550>.
- [24] C.B. Anucha, I. Altin, E. Bacaksiz, V.N. Stathopoulos, Titanium dioxide (TiO<sub>2</sub>)-based photocatalyst materials activity enhancement for contaminants of emerging concern (CECs) degradation: in the light of modification strategies, *Chem. Eng. J. Adv.* 10 (2022), 100262, <https://doi.org/10.1016/j.cej.2022.100262>.
- [25] J. Zhao, J. Yan, H. Jia, S. Zhong, X. Zhang, L. Xu, BiVO<sub>4</sub>/g-C<sub>3</sub>N<sub>4</sub> composite visible-light photocatalyst for effective elimination of aqueous organic pollutants, *J. Mol. Catal. A Chem.* 424 (2016) 162–170, <https://doi.org/10.1016/j.molcata.2016.08.025>.
- [26] P.E. Zaruma-Arias, C.M. Núñez-Núñez, L.A. González-Burciaga, J.B. Proal-Nájera, Solar heterogenous photocatalytic degradation of methylthionine chloride on a flat plate reactor: effect of pH and H<sub>2</sub>O<sub>2</sub> addition, *Catal.* 12 (2022) 132, <https://doi.org/10.3390/catal12020132>.
- [27] M. Kawano, T. Maeda, Impact of selenite, arsenate, and silicate oxyanions on the polymorphism and precipitation rate of calcium carbonate minerals in solutions with Mg<sup>2+</sup> ions, *J. Cryst. Growth* 535 (2020) 125536, <https://doi.org/10.1016/j.jcrysgro.2020.125536>.
- [28] S.J. Armaković, S. Armaković, N.L. Finčur, F. Šibul, D. Vione, J.P. Šetrajčić, B. F. Abramović, Influence of electron acceptors on the kinetics of metoprolol photocatalytic degradation in TiO<sub>2</sub> suspension. A combined experimental and theoretical study, *RSC Adv* 5 (2015) 54589–54604, <https://doi.org/10.1039/c5ra10523d>.
- [29] J. Kelly, C. McDonnell, N. Skillen, P. Manesiotis, P.K.J. Robertson, Enhanced photocatalytic degradation of 2-methyl-4-chlorophenoxyacetic acid (MCPA) by the addition of H<sub>2</sub>O<sub>2</sub>, *Chemosphere* 275 (2021), <https://doi.org/10.1016/j.chemosphere.2021.130082>. Article ID 130082.
- [30] Z. Yin, M. Han, Z. Hu, L. Feng, Y. Liu, Z. Du, L. Zhang, Peroxymonosulfate enhancing visible light photocatalytic degradation of bezafibrate by Pd/g-C<sub>3</sub>N<sub>4</sub> catalysts: the role of sulfate radicals and hydroxyl radicals, *Chem. Eng. J.* 390 (2020), <https://doi.org/10.1016/j.cej.2020.124532>. Article ID 124532.
- [31] H. Zhang, L. Chao Nengzi, Z. Wang, X. Zhang, B. Li, X. Cheng, Construction of Bi<sub>2</sub>O<sub>3</sub>/CuNiFe LDHs composite and its enhanced photocatalytic degradation of lomefloxacin with persulfate under simulated sunlight, *J. Hazard. Mater.* 383 (2020), <https://doi.org/10.1016/j.jhazmat.2019.121236>. Article ID 121236.
- [32] B. Kordestani, R. Jalilzadeh Yengejeh, A. Takdastan, A.K. Neisi, A new study on photocatalytic degradation of meropenem and ceftriaxone antibiotics based on sulfate radicals: influential factors, biodegradability, mineralization approach, *Microchem. J.* 146 (2019) 286–292, <https://doi.org/10.1016/j.microc.2019.01.013>.
- [33] S. Zhu, M.A. Khan, T. Kameda, H. Xu, F. Wang, M. Xia, T. Yoshioka, New insights into the capture performance and mechanism of hazardous metals Cr<sup>3+</sup> and Cd<sup>2+</sup> onto an effective layered double hydroxide based material, *J. Hazard. Mater.* 426 (2022), <https://doi.org/10.1016/j.jhazmat.2021.128062>. Article ID 128062.
- [34] S. Zhu, M. Xia, Y. Chu, M.A. Khan, W. Lei, F. Wang, T. Muhmood, A. Wang, Adsorption and desorption of Pb(II) on L-lysine modified montmorillonite and the simulation of interlayer structure, *Appl. Clay Sci.* 169 (2019) 40–47, <https://doi.org/10.1016/j.clay.2018.12.017>.
- [35] W. Liu, Y. Li, F. Liu, W. Jiang, D. Zhang, J. Liang, Visible-light-driven photocatalytic degradation of diclofenac by carbon quantum dots modified porous g-C<sub>3</sub>N<sub>4</sub>: mechanisms, degradation pathway and DFT calculation, *Water Res* 151 (2019) 8–19, <https://doi.org/10.1016/j.watres.2018.11.084>.
- [36] U.G. Akpan, B.H. Hameed, The advancements in sol-gel method of doped-TiO<sub>2</sub> photocatalysts, *Appl. Catal. A Gen.* 375 (2010) 1–11, <https://doi.org/10.1016/j.apcata.2009.12.023>.
- [37] M.A. Behnajady, H. Eskandarloo, Silver and copper co-impregnated onto TiO<sub>2</sub>-P25 nanoparticles and its photocatalytic activity, *Chem. Eng. J.* 228 (2013) 1207–1213, <https://doi.org/10.1016/j.cej.2013.04.110>.
- [38] S. Rengaraj, X.Z. Li, Photocatalytic degradation of bisphenol A as an endocrine disruptor in aqueous suspension using Ag-TiO<sub>2</sub> catalysts, *Int. J. Environ. Pollut.* 27 (2006) 20–37, <https://doi.org/10.1504/ijep.2006.010451>.
- [39] Q. Wang, P. Wang, P. Xu, Y. Li, J. Duan, G. Zhang, L. Hu, X. Wang, W. Zhang, Visible-light-driven photo-Fenton reactions using Zn<sub>1-1.5x</sub>Fe<sub>x</sub>S/g-C<sub>3</sub>N<sub>4</sub> photocatalyst: degradation kinetics and mechanisms analysis, *Appl. Catal. B Environ.* 266 (2020), 118653, <https://doi.org/10.1016/j.apcatb.2020.118653>.
- [40] S. Liu, C. Lai, B. Li, C. Zhang, M. Zhang, D. Huang, L. Qin, H. Yi, X. Liu, F. Huang, X. Zhou, L. Chen, Role of radical and non-radical pathway in activating persulfate for degradation of p-nitrophenol by sulfur-doped ordered mesoporous carbon, *Chem. Eng. J.* 384 (2020), <https://doi.org/10.1016/j.cej.2019.123304>. Article ID 123304.
- [41] M. Sivakumar, P.A. Tataka, A.B. Pandit, Kinetics of p-nitrophenol degradation: effect of reaction conditions and cavitation parameters for a multiple frequency system, *Chem. Eng. J.* 85 (2002) 327–338, [https://doi.org/10.1016/S1385-8947\(01\)00179-6](https://doi.org/10.1016/S1385-8947(01)00179-6).
- [42] A.A. Abdel-Khalek, S.A. Mahmoud, A.H. Zaki, Visible light assisted photocatalytic degradation of crystal violet, bromophenol blue and eosin Y dyes using AgBr-ZnO nanocomposite, *Environ. Nanotechnol. Monit. Manag.* 9 (2018) 164–173, <https://doi.org/10.1016/j.enmm.2018.03.002>.
- [43] U. Stafford, K.A. Gray, P.V. Kamat, Photocatalytic degradation of 4-chlorophenol: the effects of varying TiO<sub>2</sub> Concentration and light wavelength, *J. Catal.* 167 (1997) 25–32, <https://doi.org/10.1006/jcat.1997.1511>.
- [44] S.P. Kamble, S.B. Swant, V.G. Pangarkar, Photocatalytic degradation of m-dinitrobenzene by illuminated TiO<sub>2</sub> in a slurry photoreactor, *J. Chem. Technol. Biotechnol.* 81 (2006) 365–373, <https://doi.org/10.1002/jctb.1405>.
- [45] M.H. Priya, G. Madras, Photocatalytic degradation of nitrobenzenes with combustion synthesized nano-TiO<sub>2</sub>, *J. Photochem. Photobiol. A Chem.* 178 (2006) 1–7, <https://doi.org/10.1016/j.jphotochem.2005.06.012>.
- [46] P. Politzer, J.S. Murray, Molecular electrostatic potentials: significance and applications, in: P.K. Chattaraj, D. Chakraborty (Eds.), *Chem. React. Confin. Syst.*, 2021, pp. 113–134, <https://doi.org/10.1002/9781119683353.ch7>.
- [47] R. Thiruvengatachari, T.O. Kwon, J.C. Jun, S. Balaji, M. Matheswaran, I.S. Moon, Application of several advanced oxidation processes for the destruction of terephthalic acid (TPA), *J. Hazard. Mater.* 142 (2007) 308–314, <https://doi.org/10.1016/j.jhazmat.2006.08.023>.
- [48] M. Sun, R. Yao, Y. You, S. Deng, W. Gao, Degradation of 4-aminophenol by hydrogen peroxide oxidation using enzyme from *Serratia marcescens* as catalyst, *Front. Environ. Sci. Eng. China* 1 (2007) 95–98, <https://doi.org/10.1007/s11783-007-0018-0>.
- [49] Q.M. Chen, C. Yang, N.K. Goh, K.C. Teo, B. Chen, Photochemical degradation of 1,3-dinitrobenzene in aqueous solution in the presence of hydrogen peroxide, *Chemosphere* 55 (2004) 339–344, <https://doi.org/10.1016/j.chemosphere.2003.11.028>.
- [50] Y. Yang, J.J. Pignatello, J. Ma, W.A. Mitch, Comparison of halide impacts on the efficiency of contaminant degradation by sulfate and hydroxyl radical-based advanced oxidation processes (AOPs), *Environ. Sci. Technol.* 48 (2014) 2344–2351, <https://doi.org/10.1021/es404118q>.
- [51] M.G. Antoniou, I. Boraei, M. Solakidou, Y. Deligiannakis, M. Abhishek, L. A. Lawton, C. Edwards, Enhancing photocatalytic degradation of the cyanotoxin microcystin-LR with the addition of sulfate-radical generating oxidants, *J. Hazard. Mater.* 360 (2018) 461–470, <https://doi.org/10.1016/j.jhazmat.2018.07.111>.
- [52] N.T.T. Nguyen, A.Q.K. Nguyen, M.S. Kim, C. Lee, J. Kim, Effect of Fe<sup>3+</sup> as an electron-transfer mediator on WO<sub>3</sub>-induced activation of peroxymonosulfate under visible light, *Chem. Eng. J.* 411 (2021), <https://doi.org/10.1016/j.cej.2021.128529>. Article ID 128529.
- [53] J. Du, Y. Wang, T. Faheem, H. Xu, J. Bao Zheng, Synergistic degradation of PNP via coupling H<sub>2</sub>O<sub>2</sub> with persulfate catalyzed by nano zero valent iron, *RSC Adv* 9 (2019) 20323–20331, <https://doi.org/10.1039/c9ra02901j>.